



DETECTION OF BREAST CANCER BY A NOVEL CISA-TOA MODEL USING MAMMOGRAMS

Poornima^{1*} H N, Ganga Holi²

Article History: Received: 21.5.2023

Revised: 06.06.2023

Accepted: 21.07.2023

Abstract

Despite its proven record as a breast cancer screening tool, mammography remains labour intensive and has recognized limitations, including low sensitivity in women with dense breast tissue. In the last ten years, Neural Network advances have been applied to mammography to help radiologists increase their efficiency and accuracy. In this research, a novel breast cancer detection framework is developed and evaluated on a medical dataset. The proposed detection and classification model passes through following five major phases: pre-processing, segmentation, feature extraction, feature selection, and classification. First, the pre-processing is performed for the given input image using the median filtering technique. Then, the pre-processed image is subjected to segmentation via K-means clustering. Local Binary Pattern, Haralick Features, Contrast, Correlation, Sum of squares: Variance, Inverse Difference Moment, Entropy, Information measures, Gray Level Run Length Features are extracted. Finally, the classification process is carried out via a hybrid classification approach, which is constructed by blending the deep belief network and neural network. Experimental results demonstrate that the model is a powerful tool for diagnosing breast cancer by means of classifying the mammogram images with overall sensitivity of 1 and 0.99 AUC. To enhance the accuracy of detection, the activation function of DBN is optimized using a new Customized Individual Activity and Information Sharing based Team Work Optimization (CISA-TOA) model. This CISA-TOA is the conceptual improvement of the standard Teamwork Optimization Algorithm (TOA). Finally, a comparative evaluation is carried out to validate the efficiency of the projected model.

Keywords: Breast cancer, Computer Aided Diagnosis, Image Processing, Deep Neural Network, Artificial Intelligence, Machine Learning, Image Classification Nomenclature.

^{1*,2}Department of Information Science and Engineering, AMC College of Engineering, Bengaluru.

Email: ^{1*}puni27@gmail.com, ²gangaholi@gmail.com

DOI: 10.31838/ecb/2023.12.s3.731

Abbreviation	Description
WHO	World Health Organization
APPDRC	Altered Phase Preserving Dynamic Range Compression
ABUS	Automated Breast Ultrasound
HC	Hybrid Classification Model
DLXGB	Deep Learning And Extreme Gradient Boosting
LOA	Lizard Optimization Algorithm
BC	Breast Cancer
CNN	Convolutional Neural Network
ASM	Angular Second Moment
PCA	Principal Component Analysis
TOA	Teamwork Optimization Algorithm
SRLGE	Short Run Low Gray-Level Emphasis
DFA	Discriminant Function Analysis
GLCM	Gray Level Co-Occurrence Matrix
HGRE	High Gray-Level Run Emphasis
RERNN	Recalling Enhanced Recurrent Neural Network
NN	Neural Network
SRHGE	Short Run High Gray-Level Emphasis
ELBP	Entropy Based Local Binary Pattern
CISA-TOA	Customized Individual Activity And Information Sharing Based Team Work Optimization
LSP	Local Binary Pattern
ML	Machine Learning
AI	Artificial Intelligence
SVM	Support Vector Machines
DL	Deep Learning
CNN	Convolutional Neural Networks
RP	Run Percentage
CISA-TOA	Customized Individual Activity And Information Sharing Based Team Work Optimization
LGRE	Low Gray-Level Run Emphasis
CISA-TOA+HC	Customized Individual Activity and Information Sharing based Team Work Optimization with Hybrid Classifier

1. Introduction

The human body is made up of billions of cells [1] [2] [3] [4]. When these cells divide improperly or uncontrollably, the term “cancer” pertains to take place. Cancer may take place at any part of the body, and based upon its location, the kind of sickness is determined [5] [6] [7]. As the infection spreads to other body regions, this would result in death. BC is the most common kind of cancer reported for most women across the globe. Breast carcinoma is the most prevalent disease in women, according to the WHO,

impacting 2.1 million people each year [8] [9] [10] [11]. The phrase "BC" refers to a malignant tumor that has arisen from cancerous cells in the breast and threatens the patient's health. The risk of BC is determined by its various phases. BC has a decreased risk when cancer is discovered, but no cancerous cells have become evident in the lymphatic system. Whenever cancer cells from the breast tissue secede and are transferred to surrounding lymph nodes by the lymph fluid, there is a significant chance of mortality (fluids that gather waste products and drain into veins to be removed). BCs are classified

as benign (non-cancerous) or malignant (cancerous/metastasizing) [12] [13] [14] [15] [16]. Modifications in normal breast parenchyma tissue unrelated to the development of cancer are referred to as benign tissue. Malignant tissue, on the other hand, is categorized into two kinds: in-situ carcinoma and invasive carcinoma [17] [18] [19] [20] [21] [22]. Early identification of BC allows for efficient treatment. As a result, having access to good diagnostic techniques is critical for recognizing BC's early symptoms. Mammography, ultrasonography, and thermography are three common imaging modalities used to test this condition. Mammography is one of the most important early BC detection tools. Because mammography is ineffective for substantial breasts, ultrasound or diagnostic sonography procedures are often employed. Radiography radiations can avoid small masses, and thermography may be more efficient than ultrasonography in identifying smaller malignant tumors [2] [23] [24] [25] [26]. Mammograms can be performed to look for signs and symptoms of BC. A mammogram is an X-ray photograph of a woman's breasts. Screening mammography is performed when a woman has no symptoms of BC. BC fatalities among women between the ages of 40 and 70 can be reduced with this method. There are a few drawbacks to this method [27] [28] [29]. Breasts can sometimes go unnoticed until mammography reveals a problem. Because additional tests were conducted, this generated worry. Younger women with BC symptoms are given mammograms. Instruments have been created to make and enhance image processing because of the inherent challenges connected with images, such as low contrast, noise, and lack of appreciation by the eye. AI, ML, and CNN are now the fastest-growing fields in the healthcare business [1, 3–6]. AI and ML are two fields of research that deal with and enhance technology systems to accomplish complicated tasks by decreasing the need for human intellect [7] [8] [9]. When the training data isn't represented, the Naive Bayes Classifier gives bad results [10] [30]

[31]. The SVM classifier is ineffective on huge datasets and advanced computer vision applications. Bi-clustering and Ada boost Techniques will result in incorrect classification when the data is unbalanced. The training of an RCNN network takes longer. For BUS images, HA-BiRNN might give incorrect results [9]. The suggested technique is described in light of these constraints. Artificial neural networks were used to support DL, a subset of machine learning. Optimization and deep learning are suggested as one-stop solutions to enhance detection accuracy. These new technologies can increase cancer detection diagnostic accuracy and efficiency [13].

The major contribution of this research work is:

- Construct a new hybrid classification model (HC) with an optimized DBN and NN to classify the input images precisely as normal, benign, or malignant.
- To enhance the detection accuracy of DBN, the weight and activation function of DBN is tuned by the Customized Individual Activity and Information Sharing based Team Work Optimization (CISA-TOA) model.

The remainder of this study is arranged as follows: part II highlights current BC diagnostic research. The suggested early BC diagnosis, pre-processing using median filtering, and segmentation with K-MEANS clustering are depicted in Sections III, IV, and V, respectively. In addition, Section VI demonstrates feature extraction: LBP, Haralick, and GLRM, while Section VII explains the BC diagnostic phase: DBN with Customized Individual Activity and Information Sharing based Team Work Optimization (CISA-TOA) model. The outcomes of the conscious effort are presented in Section VIII. Finally, section IX brings the paper to a close.

Literature Review

Related Works: Bhowal Et Al. [1] Established A Novel BC Classification

Framework For Categorizing Histological Images In 2021 By Combining “VGG16, VGG19, Xception, Inception V3, And Inceptionresnet V2”. The Dataset For The "ICIAR 2018 Grand Challenge On BC Histology (Also Known As BACH) Images" Has Been Verified, And “Choquet Integral, Coalition Game Theory, And Information Theory Approaches” Have Been Used. The Predicted Model Has The Highest Test Accuracy, With A Score Of 91 Percent. On The Other Side, The Time It Takes To Identify Anything Is Longer, And The Accuracy And Recall Values Are Lower. Zhang et al. [2] used a combination of ML and Raman spectroscopy methods” to classify BC in 2021. The authors obtained Raman spectra from cultivated BC cell lines and then used PCA–DFA to analyze the data. The anticipated model exhibited 92 percent detection accuracy. Liew et al. [3] have projected DLXGB for BC classification in histopathology BC images in 2021. At first, the data was pre-processed via data augmentation and stain normalization, and then the features were extracted using the DenseNet201 and powerful gradient boosting classifier. The images were classified as binary benign and malignant and additionally one of eight non-overlapping/overlapping categories: (“Adenosis (A), Fibroadenoma (F), Phyllodes Tumour (PT), And Tubular Adenoma (TA) Ductal Carcinoma (DC), Lobular Carcinoma (LC), Mucinous Carcinoma (MC), and Papillary Carcinoma (PC)”).

Subasree et al. [4] forecast a novel technique for BC classification in 2021, based on RERNN and LOA. After pre-processing the raw data with APPDRC, radiomic characteristics such as morphologic features, grayscale statistic features, and Haralick texture features were retrieved using ELBP”. For classification, the RERNN classifier with LOA was used. The predicted model reported the maximum accuracy, which was 45.75 percent. Wang et al. [5] used a CNN to diagnose BC in ABUS imaging in 2020. To achieve effective feature extraction in ABUS

imaging, the suggested CNN uses a modified Inception-v3 architecture. The suggested CNN, which uses a multiview technique to diagnose BC, showed potential and might be utilized as a second reviewer to improve diagnostic reliability.

Problem Statement

With the growth of data mining in information systems, decision trees are authoritative classification algorithms that are becoming increasingly popular. Trees may be expressed as a series of if-then rules in this technique, which improves human readability. However, because the training data set is traversed frequently, over-fitting in the decision tree method results in misclassification error, and tree building is a task-consuming and computationally costly process. The NN is a popular AI technology that can learn data and build weight matrices to reflect the learning patterns. The main benefit of this approach is that it automatically handles noise and unexpected conditions through data generalization and allows for quick identification and categorization of incoming data. On the other hand, they are a black-box approach, which means that the relationship between a neural network and the issue it represents is difficult to comprehend. SVM is today's most powerful categorization method in terms of predicted accuracy. An SVM's answer is global and one-of-a-kind. The main disadvantage is that they produce black-box models. On the other hand, a Bayesian network is a strong tool for describing the uncertainty and complexity of many real-world issues, with a mathematical foundation that is logically explained. The model's main flaw is that missing values of an attribute cause misunderstanding.

Proposed Early BC Diagnosis

Proposed Architecture: According to global statistics, breast cancer (BC) is one of the most frequent malignancies among women globally, accounting for most new cancer cases and cancer-related deaths, making it a

major public health issue in today's society. Early detection of BC improves the prognosis and chances of survival by allowing patients to receive timely clinical treatment. Patients may avoid unneeded therapies if benign tumors are classified more precisely. As a result, accurate BC diagnosis and categorization of individuals into malignant or benign groups is a hot research topic. ML is widely regarded as the choice approach in BC pattern classification and forecast modeling due to its unique benefits in detecting essential characteristics from complicated BC datasets. The use of classification and data mining technologies to categorize data is quite successful. Particularly in the medical profession, those approaches are frequently utilized in diagnosis and analysis. Therefore, a novel BC detection model is developed in this research work. The predicted BC detection model comprises four primary phases: “pre-processing, segmentation, feature extraction, and BC classification”. The median filtering approach is used to pre-process the supplied input image img^{inp} at first. The pre-processed

image is denoted as img^{pre} . In reality, a nonlinear filter called a median filter effectively removes salt and pepper noise. While removing noise, the median keeps the clarity of image edges. The segmentation of the pre-processed image is done using K-means clustering. The K-Means clustering approach is a simple and efficient way to cluster data. The clustered image is denoted as $img^{cluster}$. Subsequently in the feature extraction stage, the features like (i) LBP f^{LBP} , (ii) Haralick Features f^{Har} (ASM, Contrast, Correlation, Sum of squares: Variance, Inverse Difference Moment, Entropy, Information measures of Correlation-I and Information measures of Correlation-II as well), (iii) Gray Level Run Length Features f^{GLRM} is extracted. Finally, the classification process is carried out via a hybrid classification approach, which is constructed by blending the DBN and NN. To enhance the accuracy of detection, the activation function of DBN is optimized using a CISA-TOA. This CISA-TOA is the conceptual improvement of standard TOA)

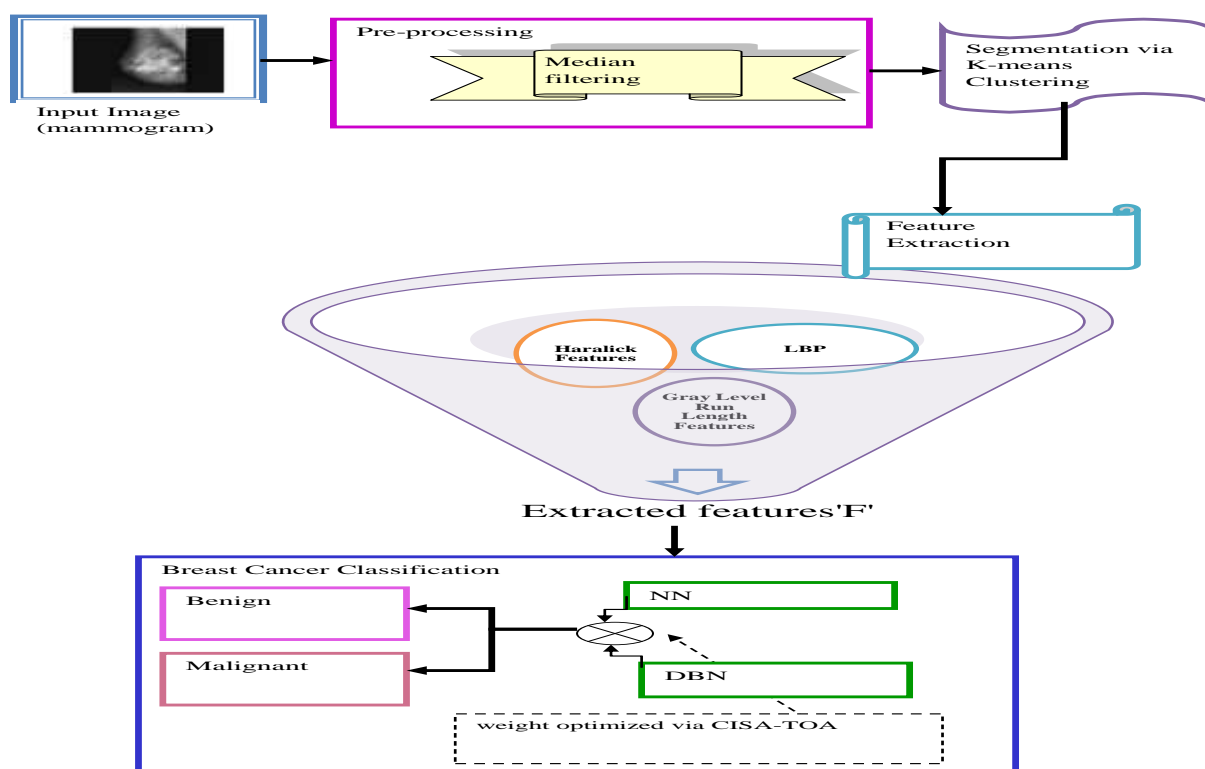


Fig. 1. The architecture of the proposed work

Pre-Processing via Median Filtering

The collected mammogram images (input image) img^{imp} are initially subjected to pre-processing phase. The main goal of using the pre-processing procedure is to improve the quality of mammography images so that more accurate findings may be obtained. In this research work, the noise available img^{imp} is removed using the median filtering approach. As a consequence, img^{imp} is sharpened (i.e., image edges and boundaries are sharpened).

Median Filtering

The median filtering [32] is the most renowned filtering for suppressing the random noise from the image. The median filtering mechanism moves a window across the input image $img^{imp}(a,b)$ the center pixel of the image is replaced by the corresponding median value of the window—the median value for the input image $img^{imp}(a,b)$ as per Eq. (1). The pre-processing image acquired at the end of median filtering is denoted as img^{pre} , which is fed as input to the segmentation phase.

$$img^{pre} = med \{img^{imp}(a-j, b-k) | j, k \in T\} \quad (1)$$

Here, T and j , as well, represents the image pixels in a 2-D mask of size $n \times n$. The pre-processed image is denoted as img^{pre}

Segmentation via K-Means Clustering

K-means Clustering: The segmentation is the mechanism of finding the ROI of img^{pre} . The image segmentation process adds extra meaning to the image. Here, the region with the tumor landmarks is grouped using the K-means clustering model [33].

The K-means is an unsupervised learning model that segments the region of interest from the background. It is the most commonly utilized clustering model, and here K denotes the count of clusters.

The working principle behind the K-means model is manifested below:

Step 1: The count of clusters are pre-defined (i.e. K-value)

Step 2: To every cluster, the data points of img^{pre} are assigned randomly.

Step 3: Then, the cluster centers are computed.

Step 4: The data points distance is computed from each of every cluster.

Step 5: Reassign the data points to the clusters closest to them, based on their distance from the cluster.

Step 6: The new cluster center is calculated once more.

Step 7: Steps 4-6 are repeated until no data points change their clusters.

The clustered images is denoted as $img^{cluster}$

Feature Extraction: LBP; GLRM; Haralick

In the feature extraction stage, the features like “(i) LBP, (ii) Haralick Features (Angular Second Moment (ASM), Contrast, Correlation, Sum of squares: Variance, Inverse Difference Moment, Entropy, Information measures of Correlation-I and Information measures of Correlation-II as well), (iii) Gray Level Run Length Features” are extracted for each of the data points available in the clusters $img^{cluster}$.

LBP

The LBP [34] is a useful texture descriptor used to threshold nearby pixels based on their current pixel value. It is significant in capturing the grayscale contrast and the local spatial patterns from the image. In this research work, the LBP features are extracted $img^{cluster}$ by following the four major steps furnished below:

Step 1: In $img^{cluster}$, for each of the pixels (a,b) , the neighboring pixels are chosen at a radius R

Step 2: The difference in intensities is computed for the current pixels (a,b) with the intensities of the neighboring pixels Q

Step 3: Create a bit vector by throttling the intensity difference so that all negative differences are given 0, and all positive differences are assigned 1.

Step 4: Convert the P-bit vector to its corresponding decimal value and replace the intensity value at (x,y) with this decimal value.

Thus, the LBP descriptor for every pixel is given as

$$f^{LBP} = LBP(a,b) = \sum_{q=0}^Q f(\text{pix}_Q - \text{pix}_C)$$

Here, pix_Q and pix_C denotes the intensities of the neighboring and current pixels,

respectively. The extracted LBP feature is denoted as f^{LBP} .

Haralick Features

A GLCM, a matrix that counts the co-occurrence of nearby grey levels in an image, is used to determine Haralick texture characteristics. The GLCM is a square matrix with a dimension equal to the number of grey levels N in the target region (ROI). In general, this GLCM in image data is used to create a matrix co-occurrence, wherein the features matrices function may be obtained. The extracted GLCM feature is denoted as f^{Har} . The heraldic features are listed in Table II.

Haralick features

Parameter	Mathematical formula
Variance	$Va = \sum_A \sum_B (A - \mu)^2 E_{AB}$ Where, $\mu \rightarrow$ mean of E_{AB}
Sum Variance	$SV = \sum_{A=2}^{2N_G} (A - SE)^2 H_{A,B}(A)$
Sum Entropy	$SE = \sum_{x=2}^{2N_G} H_{x+y}(x) \log\{E_{x+y}(x)\}$
Sum Average	$SA = \sum_{A=2}^{2N_G} A.E_{A+B}(A)$ Where $N_G \rightarrow$ varied gray levels in image.
MCC (2 nd higher Eigen value of Q) ^{0.5}	$MCC = \sum_y \frac{E(A,y)E(B,y)}{E_A(A)E_B(B)}$
IMC1	$IMC1 = \frac{ABC - ABC1}{\max\{AB, AC\}}$
IMC 2	$IMC2 = \sqrt{(1 - \exp[-2.0[ABC2 - ABC]])}$ where $ABC = -\sum_R \sum_S H_{RS} \log_2 H_{RS}$ $ABC1 = -\sum_R \sum_S H_{RS} \log_2 \{H_R(R)H_S(S)\}$ $ABC2 = -\sum_A \sum_B E_A(A)E_B(B) \log_2 \{E_A(A)E_B(B)\}$
Homogeneity	$H = \sum_A \sum_B \frac{1}{1 + (A - B)^2} E_{AB}$
Entropy	$Ent = -\sum_A \sum_B H_{AB} \log_2 E_{AB}$
Energy	$Energy = \sum_A \sum_B E_{AB}^2$ $E_{AB} \rightarrow (A < B)^{th} \text{ entry in } I^{seg}$
Difference Variance	$DV = \text{variance of } E_{A-B}$
Difference Entropy	$DE = \sum_{A=0}^{N_G-1} H_{A-B}(A) \log\{E_{A-B}(A)\}$

Correlation	$C = \frac{\sum_A \sum_B (AB) E_{AB} - \mu_A \mu_B}{\sigma_A \sigma_B},$ <p>where $\sigma_A, \sigma_B \rightarrow$ std deviations of H_A, H_B</p> <p>$\mu_A, \mu_B \rightarrow$ mean of H_A, H_B</p>
Contrast	$Con = \sum_A \sum_B (A - vB)^2 E_{AB}$

GLRM

Here, the geometric features are represented in the form of a matrix. The pixel intensity is measured along the specified direction, as run length. In the image, each object is depicted

with the count of objects t with intensity v along the specified direction δ . The count of pixels in the run is said to be run length. The GLRM [35] features f^{GLRM} are depicted in Table II.

GLRM features

Features	Mathematical Expression
HGRE (HG^{RE})	$HG^{RE} = \frac{1}{d_r} \sum_{v=1}^S \sum_{t=1}^D P(v,t) * v^2$
LGRE (LG^{RE})	$LG^{RE} = \frac{1}{d_r} \sum_{v=1}^S \sum_{t=1}^D \frac{P(v,t)}{v^2}$
SRLGE (SRL^{GE}):	$SRL^{GE} = \frac{1}{d_r} \sum_{v=1}^S \sum_{t=1}^D \frac{P(v,t)}{v^2 * t^2}$
SRHG	$SRH^{GLE} = \frac{1}{d_r} \sum_{v=1}^S \sum_{t=1}^D \frac{P(v,t).t^2}{t^2}$
RP	$RP = \frac{d_r}{d_p}$ <p>Here, overall counts of observed runs d_r to the count of the possible runs d_p.</p>

The extracted feature set is denoted as $f^{GLRM} + f^{LVP} + f^{Har} = F$. Using F the NN and DBN in breast cancer classification framework is trained.

BC diagnosis phase: NN and DBN with Customized Individual Activity and Information Sharing based Team Work Optimization (CISA-TOA)

Hybrid Classifier

This research work constructs a hybrid classifier by blending the NN and optimized DBN model. First, both classifiers are trained parallel with the extracted feature F . Then, the outcome from NN out^{NN} and optimized DBN out^{DBN} are combined by computing the average value $out = (out^{DBN} + out^{NN})/2$ of the acquired outcome.

Optimized DBN

Smolensky introduced DBN [36] with numerous layers in the year 2018. The input layer contains visible neurons, whereas the

output layer contains hidden neurons. There is an exclusive and symmetric link between the hidden and visible neurons. Furthermore, there is no link between the input neurons and the hidden neurons, which is a specific property of DBN. The Boltzmann networks with stochastic neurons produce the result (y), which is probabilistic and has a probability function $pf(\psi)$ according to Eq. (2). Furthermore, Eq. (3), where t is the pseudo-temperature that changes the stochastic model into a deterministic model when it hits 0, is the mathematical formula for $pf(\psi)$. Boltzmann machine (Boltzmann machine): The energy of the Boltzmann machine is computed in the configured neuron state \hat{s} , as shown in Eq. (5). $w_{x,y}$ is the weight between neurons x and y , whereas θ_x and \hat{s}_x denote the biases binary states of neurons, respectively.

$$pf(\psi) = \frac{1}{1 + e^{-\frac{\psi}{t}}} \quad (2)$$

$$y = \begin{cases} 0 & \text{with } 1 - pf(\psi) \\ 1 & \text{with } pf(\psi) \end{cases} \quad (3)$$

$$\lim_{t \rightarrow 0^+} pf(\psi) = \lim_{t \rightarrow 0^+} \frac{1}{1 + e^{-\frac{\psi}{t}}} = \begin{cases} 0 & \text{for } \psi < 0 \\ \frac{1}{2} & \text{for } \psi = 0 \\ 1 & \text{for } \psi > 0 \end{cases} \quad (4)$$

$$En(\hat{s}) = -\sum_{x < y} \hat{s}_x \hat{s}_y W_{x,y} - \sum_x \theta_x \hat{s}_x \quad (5)$$

Eq. calculates the impact of a single unit state \hat{s}_x on global energy. The gradient descent mechanism in the system assists in discovering the lowest feasible energy in the training process for the given input.

$$\Delta En(\hat{s}_x) = \sum_y \hat{s}_y W_{x,y} + \theta_x \quad (6)$$

Restricted Boltzmann Machine (RBM): It is not the same as a regular Boltzmann Machine. The main distinction is that RBM does not compute the energy difference between visible and hidden neurons using visible or hidden neurons. The energy definitions of visible and hidden neurons

linked to joint composition are represented by Eqs. (7), (8), and (9).

$$En(\vec{c}, \vec{d}) = -\sum_{(x,y)} W_{x,y} c_x d_y - \sum_x c_x a_x - \sum_y d_y p_y \quad (7)$$

$$\Delta En(c_x, \vec{d}) = \sum_y W_{xy} d_y + a_x \quad (8)$$

$$\Delta En(\vec{c}, d_y) = \sum_x W_{xy} c_x + p_y \quad (9)$$

The visible unit x 's binary state and bias are designated as c_x and a_x , respectively. The notation denotes the weight of the neurons $w_{x,y}$. The hidden unit y 's binary state and bias are also represented as d_y and p_y , respectively.

RBM training: For RBM training, unsupervised learning is used. The training model helps to improve the probabilities given to the training set Z , and the maximal probability may be calculated using the weight assignment Wt_m , as indicated in Eq. (10). RBM, represented in Eq. (10), then assigns the probability to every pair of visible and hidden neurons using the energy function specified in Eq. (7). (11). the sum of the energies of all conceivable states is known as the partition function, written as Eq. (12).

$$Wt_m = \max_{Wt} \prod_{\vec{c} \in Z} pf(\vec{c}) \quad (10)$$

$$pf(\vec{c}, \vec{d}) = \frac{1}{Ji} e^{-En(\vec{c}, \vec{d})} \quad (11)$$

$$Ji = \sum_{\vec{c}, \vec{d}} e^{-En(\vec{c}, \vec{d})} \quad (12)$$

The loss function $Loss()$ ought to be minimized to achieve higher classification accuracy. This minimization of the loss function is the major objective behind this research work. The objective function is mathematically given in Eq.(13).

$$Obj = \min[Loss()] = Loss() = RMSE \quad (13)$$

Contrastive Divergence (CD) is a learning approach for initializing visible states that does not require that the visible states be

initialized at random. Instead, CD uses input data to establish the visible states and then reconstructs the model predictions from the input data. The steps of the CD algorithm are summarised in the following sections.

1. Samples for training c have been chosen and are braced against the observable states.
2. The probability of concealed neurons is denoted by the letter P, which is obtained by multiplying c (visible vector) by w_t (weight matrix) as $pf_d = \chi(c.Wt)$ in Eq. (14).

$$pf(d_y \rightarrow 1 | \vec{c}) = \chi\left(p_y + \sum_x c_x W_{t,x,y}\right) \quad (14)$$

3. The hidden states c are then sampled using the gained probability pf_d .
4. The outer product, or positive gradient ϕ^+ , is calculated by multiplying c (visible vector) by pf_d (probability of hidden neurons) as per $\phi^+ = c.pf_d^T$
5. Furthermore, the reconstruction of visible states c' takes place from d (hidden vector), while the reconstruction of

hidden states d' takes place from c' (visible states).

$$pf(c_x \rightarrow 1 | \vec{d}) = \chi\left(a_x + \sum_y d_y W_{t,x,y}\right) \quad (15)$$

6. The negative gradient ϕ^- , also known as the outer product, is calculated by multiplying c' and d' according to $\phi^- = c'.d'^T$.
7. The weight updates $\Delta W_t = \eta(\phi^+ - \phi^-)$ are determined by subtracting the calculated positive and negative gradients ϕ^+ and ϕ^-
8. The weights are also updated with the newly acquired values as $W'_{t,x,y} = W_{t,x,y} + \Delta W_{t,x,y}$

One of the most well-known gradient approximations for RBM is CD. In DBN's architecture, RBM and MLP layers are provided. In MLP, supervised learning is used, while in RBM, unsupervised learning is used. The weight of DBN is optimized using CISA-TOA, and the solution encoding (i.e. weight function) fed as input is shown in Fig.2.

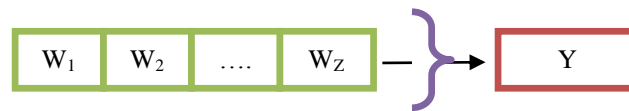


Fig. 2. Solution Encoding

NN:

NN [37] absorbs the extracted features and displays the presence or absence of a BC. NN is made up of three main layers: input, output, and hidden. Eqs. (16) and (17) express the NN network model analytically (16). $hid = 1, 2, \dots, N_{hid}$ hidden neurons hid are found in the hidden layer. The output neuron (out) is located in the output layer where $out = 1, 2, \dots, N_{out}$. In addition, there are input neurons inp in the input layer, where $inp = 1, 2, \dots, N_{inp}$. hid and out 's bias weights are denoted by $wg_{b,hid}^N$ and $wg_{b,out}^{r*}$, respectively. $wg_{inp,hid}^N$ and $wg_{hid,out}^{r*}$ are the weights from inp to hid and hid to out , respectively. The error function is the

difference between (actual outputs) and (expected outputs) $F(er)$. The overall features extracted F and $N^? \hat{n}$ indicate the count of features. The notation A_{fun} in Eq. (16) and Eq. (17) is the activation function. The mathematical formula for hidden layer Hid is depicted in Eq. (18).

$$Hi = A_{fun}\left(wg_{b,hid}^N + \sum_{inp=1}^{N_{inp}} wg_{inp,hid}^N f^{feat}\right) \quad (16)$$

$$Pr = A_{fun}\left(wg_{b,out}^{r*} + \sum_{hid=1}^{N_{hid}} wg_{hid,out}^{r*} Hi\right) \quad (17)$$

$$F(er) = \arg \min_{\{wg_{b,hid}^N, wg_{inp,hid}^N, wg_{b,out}^{r*}, wg_{hid,out}^{r*}\}} \sum_{out=1}^{N_{out}} |Ac - Pr| \quad (18)$$

CISA-TOA

This research work introduces a new optimization model called Customized Individual Activity and Information Sharing based Team Work Optimization (CISA-TOA) to fine-tune the DBN weight. This CISA-TOA is an improved version of the standard TOA model; In reality, the TOA model was created to address team members' cooperation behaviors to attain their intended aim. The TOA model is good for solving optimization problems and providing quasi-optimal solutions. However, even though the TOA [38] is highly convergent, it sometimes gets stuck within the local optima. Therefore the global best solutions couldn't be acquired. Therefore, in this research work, the information sharing and individual activity phases of TOA are customized to enhance the convergence speed of the solutions. The steps followed in CISA-TOA model is furnished below:

Step 1: The count of team members (search agents) (M), as well as iterations, Max^{itr} is set.

Step 2: Randomly generate the initial population matrix

Step 3: The objective function is computed for every search agent using Eq. (13).

Step 4: For $itr=1:Max^{itr}$ do

Step 5: The supervisor is updated as per Eq. (14).

Step 6: For $i=1:M$ do

(a) Supervisory guidance: The initial phase involves updating team members according to supervisory directions. The supervisor now shares their expertise and reports with the rest of the team, directing them toward the desired outcome.

Eqs. (14)- (16) are used to update the position of the search agent accordingly.

$$X_i^{S1} : x_{i,d}^{S1} = x_{i,d} + rand * (S_s - I * x_{i,d}) \quad (14)$$

$$X_i = \begin{cases} X_i^{S1} & Obj_i^{S1} < Obj_i \\ X_i & else \end{cases} \quad (15)$$

$$I = round(1 + rand) \quad (16)$$

Here, X_i^{S1} denotes the new status of the team member i under the supervisor's guidance. In addition, Obj_i^{S1} is the defined objective function and $x_{i,d}^{S1}$ is the new value of i^{th} search agent for the d^{th} problem. Finally, the update index value is denoted as I a random value generated between intervals $[0,1]$.

(b) Information sharing: In the second stage, each team member seeks to enhance their performance by using the information of other team members who have done better than them. Our contribution resides in this phase. First, the better team members are identified and determined for team members. This computation is undergone concerning Eq. (17). Then, X_i the newly projected mathematical model is updated in Eq. (18) and Eq. (19), respectively.

$$X^{N,i} : x_d^{N,i} = \frac{\sum_{j=1}^{M_i} x_{j,d}^{g,i}}{M_i} \quad (17)$$

$$X_i^{S2} : x_{i,d}^{S2} = x_{i,best} + rand * (x_d^{N,i} - I * x_d) * sign(Obj_i - Obj_i^{N,i}) \quad (18)$$

$$X_i = \begin{cases} X_i^{S2} & Obj_i^{S2} < Obj_i \\ X_i & else \end{cases} \quad (19)$$

Here, $X^{N,i}$ denotes the mean value of the team member that's better than team member i . In addition, $Obj_i^{N,i}$ is the objective function and M_i is the team members' count that is better than i^{th} search agent and X_i^{S2} denotes the new status of the team member. Moreover, $x_{i,best}$ is the best search agent that has been newly considered in this research work for convergence enhancement.

In addition, $x_d^{N,i}$ is computed using the newly projected expression shown in Eq. (20).

Here, the geometric mean is computed for the search agents.

$$x_d^{N,i} = \left(\prod_{j=1}^{M_i} x_{j,d}^{g,i} \right)^{1/M_i} \quad (20)$$

(c) Individual activity: At this level, each team member attempts to better their

performance based on her or his current circumstances. In this period, too, we have a role to play. As stated in Eqs. (21) and (22) correspondingly, a new mathematical model is established.

$$X_i^{s3} : x_{i,d}^{s3} = x_{i,best} + (-0.01 + r * 0.02) * x_{i,d} \quad (21)$$

$$X_i = \begin{cases} X_i^{s3} & Obj_i^{s3} < Obj_i \\ X_i & else \end{cases} \quad (22)$$

Here r is a random value generated using the sinusoidal chaotic map, and this generation of the random value is the newly contributed one.

Here, X_i^{s3} denotes the new status of the team member based on the 3rd stage and Obj_i^{s3} is the objective function.

Step 7: End for $i=1:M$ $itr=1:Max^{itr}$

Step 8: Save the acquired best solution acquired so far

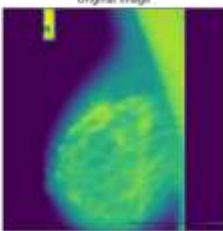
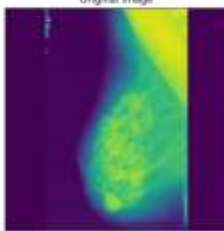
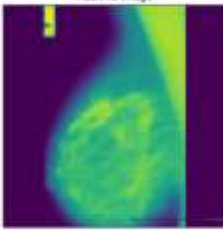
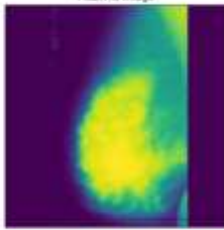
Step 9: End For $itr=1:Max^{itr}$

Step 10: Return the best solution

Step 11: Terminate

2. Results and Discussions

Experimental Setup: In PYTHON, the proposed model was implemented. MIAS Database was used to assess the suggested work (CISA-TOA+HC). The original MIAS Database (digitized at 50 micron pixel edge in [31]) has been lowered to 200-micron pixel edge and clipped/padded such that each image is 1024 x 1024 pixels. The proposed model's algorithmic performance, convergence, and classifier assessments are all examined. Figure 3 shows the sample images, pre-processed images, and segmented images. In addition, 70% of the data was used to train the CISA-TOA+HC, with the remaining 30% being used to test the CISA-TOA+HC. The assessments were carried out at different learning rates of 60, 70, 80, and 90. Positive performance (specificity, sensitivity, precision, and accuracy), as well as negative performance (FPR, FNR) and other metrics, are used to assess the suggested classifier and method (F1-score and MCC). Positive parameters of the proposed speech emotion recognition, such as specificity, sensitivity, precision, and accuracy, should be kept as high as feasible. In contrast, negative measurements, such as FPR and FNR, should be kept as low as possible.

Image type	Benign	Malignant
original Image		
median filtering based pre-processed image		

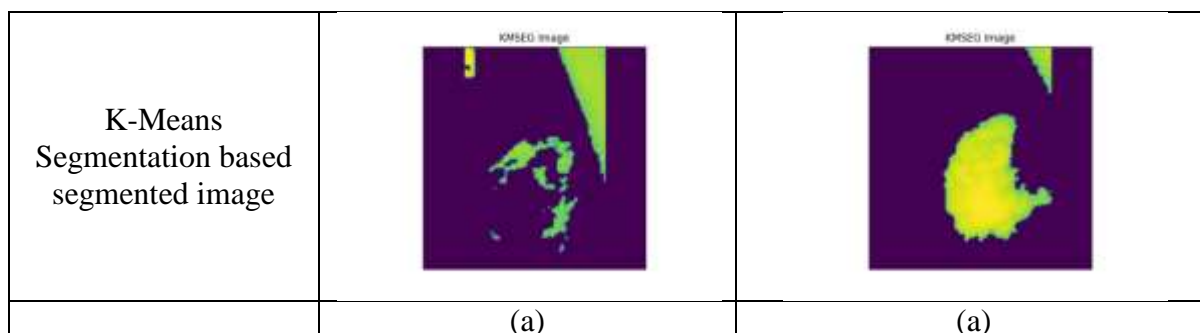


Fig. 2. Sample Images, Pre-processed and Segmented images

Performance Analysis: MIAS Database

The assessment of both the proposed work (CISA-TOA+HC) and the existing work (TOA+HC, SSA+HC, SMO+HC, and BOA+HC, respectively) are evaluated in this section. Positive Measures: Positive metrics such as “specificity, sensitivity, precision, and accuracy” are assessed, and the findings obtained are demonstrated in Fig.4. The accuracy of the CISA-TOA+HC is above 95%, while the accuracy of the existing models is much lower than that. The hybridization of NN and optimized DBN has enhanced the classification performance. The suggested CISA-TOA+HC for MIAS Database is 46.23 percent, 35.4 percent, 33.3 percent, and 22.5 percent better than classic models like TOA+HC, SSA+HC, SMO+HC, and BOA+HC at the 60th learning percentage. As a consequence of the findings, it is obvious that the suggested classifier is effective in diagnosing BC. The extraction of the LBP features and the extracted standard Haralick and GLRM features is the main cause for this improvement. All of these factors worked together to improve classification precision. Other positive indicators such as specificity, sensitivity, and accuracy are explored to add value to this study. Furthermore, the CISA-TOA+HC has

a greater specificity, sensitivity, and accuracy than previous work. As a result, the statement above that the positive measurements for the CISA-TOA+HC must be higher is proven to be true. Negative and other Measures: To demonstrate that the CISA-TOA+HC achieves the fitness function of loss reduction, the negative measures must be lower. The CISA-TOA+HC, as a powerful solution to this assertion, displays the lowest error measures for both MIAS Databases, as shown in Fig.5 and Fig.6, respectively. The CISA-TOA+HC is 66.6 percent, 75 percent, 80 percent, and 78.1 percent better than current approaches like TOA+HC, SSA+HC, SMO+HC, and BOA+HC, respectively, on the 60th learning percentage. As a result of the entire examination, it is obvious that the CISA-TOA+HC has the lowest error measures and hence may be used to diagnose BC. Furthermore, other variables, such as F1-score, NPV, and MCC, are taken into account to strongly show that the CISA-TOA+HC is more relevant for BC diagnosis. When looking at the results of the CISA-TOA+HC for MIAS Database in terms of additional performance metrics (shown in Fig. 10 and Fig. 11, respectively), the CISA-TOA+HC achieve the greatest maximal feasible results.

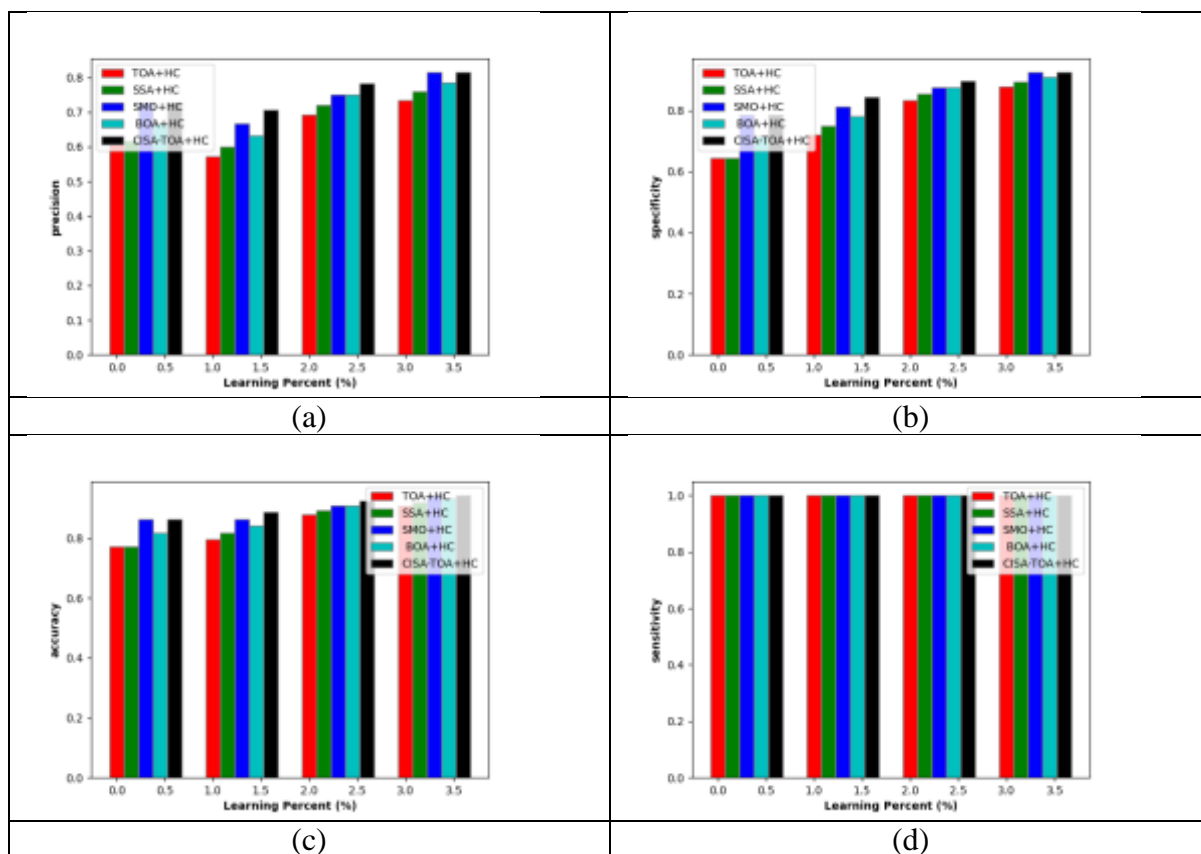


Fig. 3. Performance analysis of proposed work corresponding to (a) precision (b) specificity (c) accuracy (d) sensitivity

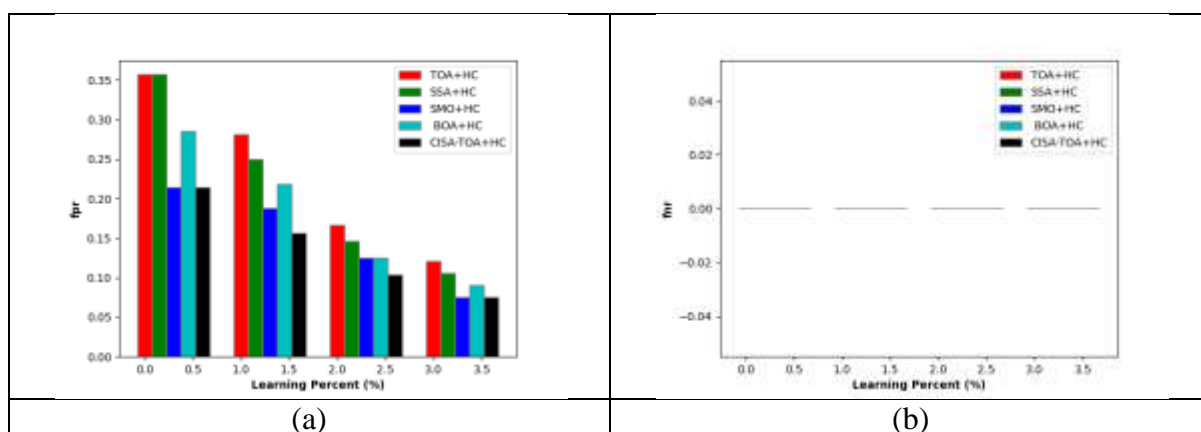


Fig. 4. Performance analysis of proposed work corresponding to (a) FPR (b) FNR

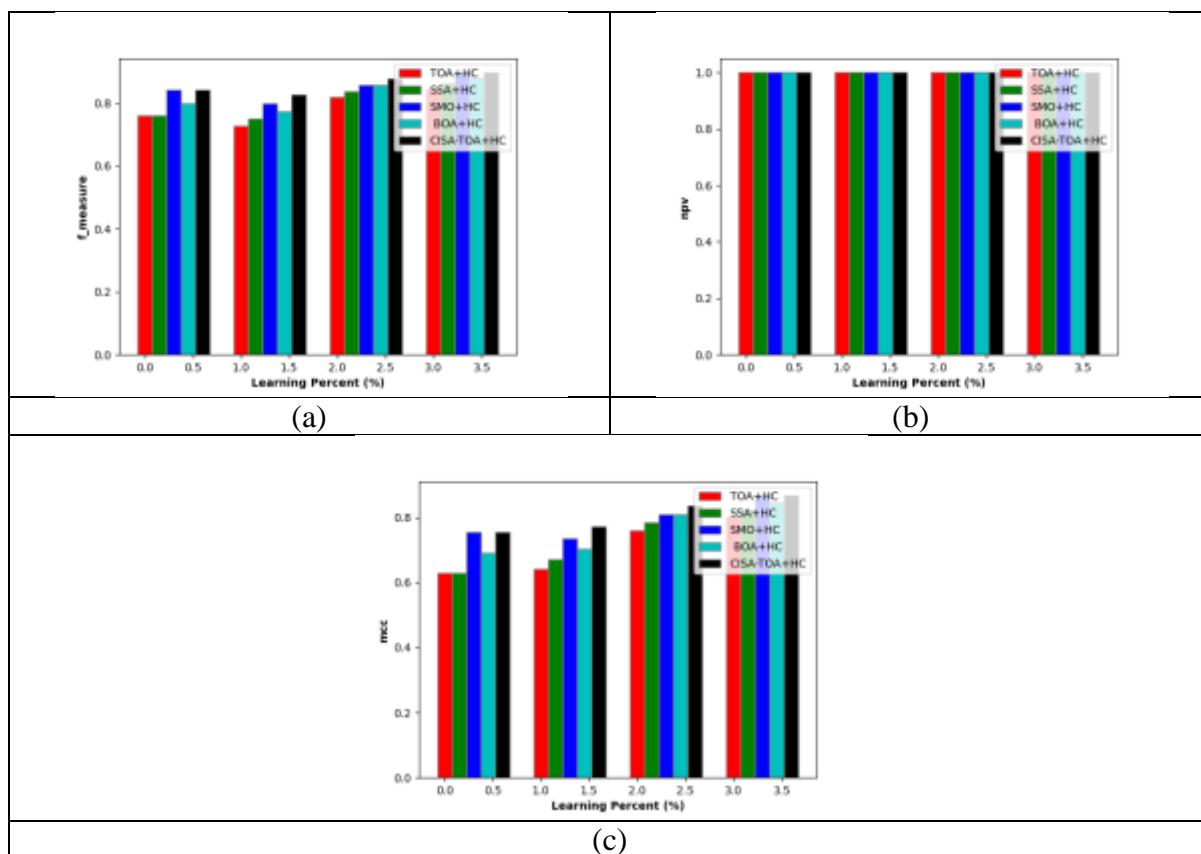


Fig.5 Performance analysis of proposed work corresponding to (a) F-measure (b) NPV (c) MCC

Overall Performance Analysis

Table III lists the findings obtained with the CISA-TOA+HC for MIAS Database corresponding to LP=70. The suggested classifier's accuracy improves for each adjustment in the learning percentage. The CISA-TOA+HC has the greatest accuracy of 0.886364 in the MIAS Database, which is superior to current approaches like

CNN=0.864865, RNN=0.891892, RF=0.864865, NB=0.810811, and NN+DBN=0.886364. Furthermore, compared to existing approaches, the negative metrics for the CISA-TOA+HC appear to be lower. As a result of the study, it is clear that the CISA-TOA+HC is quite useful for BC diagnosis.

Overall Performance Analysis of proposed work

Measures	CNN	RNN	RF	NB	CISA-TOA+HC
Accuracy	0.864865	0.891892	0.864865	0.810811	0.924242
Sensitivity	0.6875	0.75	1	0.875	1
Specificity	1	1	0.761905	0.761905	0.895833
Precision	1	1	0.761905	0.736842	0.782609
F-Measure	0.814815	0.857143	0.864865	0.8	0.878049
MCC	0.745177	0.793725	0.761905	0.631293	0.837309
NPV	0.807692	0.84	1	0.888889	1
FPR	0	0	0.238095	0.238095	0.104167
FNR	0.3125	0.25	0	0.125	0

Convergence Analysis

A convergence study (CISA) validates the suggested algorithm's efficiency. This paper presents a new optimization approach for fine-tuning the DBN's weight and activation function, which results in the final identified outcomes. The main goal of this study is to reduce DBN's RMSE performance (error performance) so that detection accuracy may be improved. The cost function confirms the provided optimization model in terms of the developed objective function. The suggested model is compared to current optimization

models such as TOA, SSA, SMO, and BOA. The outcome acquired is shown in Fig.7. According to the results obtained for the MIAS Database, the CISA's cost function is certainly larger at the lowest iteration count as the number of iterations grows, the cost functions of both the proposed and current models decreases. Moreover, for every change in LP, the cost functions of the CISA are lower than the previous models. As a result of the overall assessment, it is obvious that CISA has achieved the defined goal function.

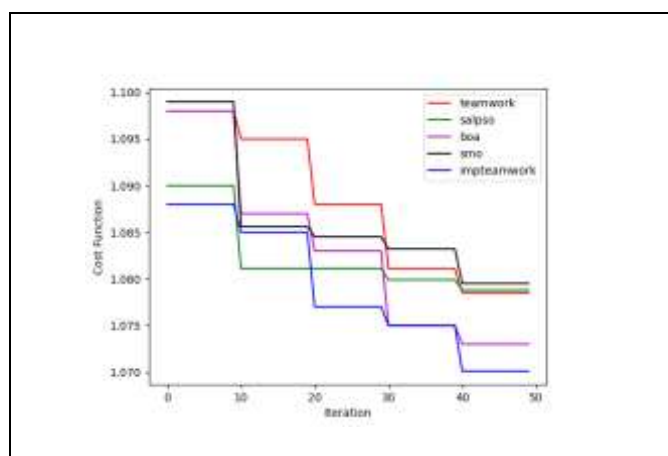


Fig. 5. Convergence Analysis of the projected model

Statistical Analysis

The CISA-TOA+HC are statistically analyzed (mean, median, standard deviation, minimal, and maximum). Table IV shows the findings obtained for the MIAS Database. Following the results, it was discovered that the CISA-TOA+HC had achieved the best results, owing to the precise categorization of

the images with optimized DBN and NN. Furthermore, as a result of the evaluation, it is clear that the CISA-TOA+HC has better average performance due to the addition of a new optimization model for fine-tuning the DBN weight.

Statistical performance of proposed work

Approaches	best	worst	mean	median	standard deviation
TOA+HC	0.090909	0.227273	0.160985	0.162879	0.056533
SSA+HC	0.079545	0.227273	0.148674	0.143939	0.058888
BOA+HC	0.068182	0.181818	0.125	0.125	0.046853
SMO+HC	0.056818	0.136364	0.105114	0.113636	0.033494
CISA-TOA+HC	0.056818	0.136364	0.095644	0.094697	0.031164

3. Conclusion

In this research, a novel BC detection framework has been developed by following

four major phases: pre-processing, segmentation, feature extraction, and BC classification. First, the pre-processing is performed for the given input image using the

median filtering technique. Median filter has been a nonlinear filter that has been efficient in removing salt and pepper noise median tends to keep the sharpness of image edges while removing noise. The pre-processed image has been subjected to segmentation via K-means clustering. The K-Means has been a technique that has been quite simple and quick clustering data. Subsequently, in the feature extraction stage, the features like “(i) LBP, (ii) Haralick Features (ASM, Contrast, Correlation, Sum of squares: Variance, Inverse Difference Moment, Entropy, Information measures of Correlation-I and Information measures of Correlation-II as well), (iii) Gray Level Run Length Features (Short Run Emphasis, Long Run Emphasis, Gray Level Non-uniformity, Run Length Non-uniformity, Run Percentage, Low Gray Level Run Emphasis has been and High Gray Level Run Emphasis)” are extracted. Finally, the classification process is carried out via hybrid classification approach, which is constructed by blending the DBN and NN, respectively. In order to enhance the accuracy of detection, the activation function of DBN is optimized using a new CISA-TOA model. This CISA-TOA has been the conceptual improvement of standard TOA. Finally, a comparative evaluation has been carried out to validate the efficiency of the projected model.

4. References

1. Pratik Bhowal, Subhankar Sen, Ram Sarkar, "Fuzzy ensemble of deep learning models using choquet fuzzy integral, coalition game and information theory for BC histology classification", *Expert Systems with Applications*, 2021
2. Lihao Zhang, Chengjian Li, Xia Huang, "Raman spectroscopy and machine learning for the classification of BCs", *Spectrochimica Acta Part A: Molecular and Biomolecular Spectroscopy*, 2021
3. Xin Yu Liew, Nazia Hameed, Jeremie Clos, "An investigation of XGBoost-based algorithm for BC classification", *Machine Learning with Applications*, 2021
4. S. Subasree, N. K. Sakthivel, Amit Kumar Tyagi, "Combining the advantages of radiomic features based feature extraction and hyper parameters tuned RERNN using LOA for BC classification", *Biomedical Signal Processing and Control*, 2021
5. Yi Wang, Eun Jung Choi, Seok-Bum Ko, "BC Classification in Automated Breast Ultrasound Using Multiview Convolutional Neural Network with Transfer Learning", *Ultrasound in Medicine & Biology*, 2020
6. X. Feng et al., "Accurate Prediction of Neoadjuvant Chemotherapy Pathological Complete Remission (pCR) for the Four Sub-Types of BC," *IEEE Access*, vol. 7, pp. 134697-134706, 2019. doi: 10.1109/ACCESS.2019.2941543
7. C. Chen, Y. Wang, J. Niu, X. Liu, Q. Li and X. Gong, "Domain Knowledge Powered Deep Learning for BC Diagnosis Based on Contrast-Enhanced Ultrasound Videos," *IEEE Transactions on Medical Imaging*, vol. 40, no. 9, pp. 2439-2451, Sept. 2021. doi: 10.1109/TMI.2021.3078370
8. P. Liu, B. Fu, S. X. Yang, L. Deng, X. Zhong and H. Zheng, "Optimizing Survival Analysis of XGBoost for Ties to Predict Disease Progression of BC," *IEEE Transactions on Biomedical Engineering*, vol. 68, no. 1, pp. 148-160, Jan. 2021. doi: 10.1109/TBME.2020.2993278
9. B. Fu, P. Liu, J. Lin, L. Deng, K. Hu and H. Zheng, "Predicting Invasive Disease-Free Survival for Early Stage BC Patients Using Follow-Up Clinical Data," *IEEE Transactions on Biomedical Engineering*, vol. 66, no. 7, pp. 2053-2064, July 2019. doi: 10.1109/TBME.2018.2882867
10. K. Park, W. Chen, M. A. Chekmareva, D. J. Foran and J. P. Desai, "Electromechanical Coupling Factor of Breast Tissue as a Biomarker for BC," *IEEE Transactions on Biomedical Engineering*, vol. 65, no. 1, pp. 96-103,

- Jan. 2018.
doi: 10.1109/TBME.2017.2695103
11. X. Li, M. Radulovic, K. Kanjer and K. N. Plataniotis, "Discriminative Pattern Mining for BC Histopathology Image Classification via Fully Convolutional Autoencoder," *IEEE Access*, vol. 7, pp. 36433-36445, 2019.
doi: 10.1109/ACCESS.2019.2904245
 12. H. M. Whitney, H. Li, Y. Ji, P. Liu and M. L. Giger, "Comparison of Breast MRI Tumor Classification Using Human-Engineered Radiomics, Transfer Learning From Deep Convolutional Neural Networks, and Fusion Methods," in *Proceedings of the IEEE*, vol. 108, no. 1, pp. 163-177, Jan. 2020.
doi: 10.1109/JPROC.2019.2950187
 13. G. Alexandrou et al., "Detection of Multiple BC ESR1 Mutations on an ISFET Based Lab-on-Chip Platform," *IEEE Transactions on Biomedical Circuits and Systems*, vol. 15, no. 3, pp. 380-389, June 2021.
doi: 10.1109/TBCAS.2021.3094464
 14. Q. Wuniri, W. Huangfu, Y. Liu, X. Lin, L. Liu and Z. Yu, "A Generic-Driven Wrapper Embedded With Feature-Type-Aware Hybrid Bayesian Classifier for BC Classification," *IEEE Access*, vol. 7, pp. 119931-119942, 2019.
doi: 10.1109/ACCESS.2019.2932505
 15. H. Lee, J. Park and J. Y. Hwang, "Channel Attention Module With Multiscale Grid Average Pooling for BC Segmentation in an Ultrasound Image," *IEEE Transactions on Ultrasonics, Ferroelectrics, and Frequency Control*, vol. 67, no. 7, pp. 1344-1353, July 2020.
doi: 10.1109/TUFFC.2020.2972573
 16. U. M. Pal et al., "Towards a Portable Platform Integrated With Multispectral Noncontact Probes for Delineating Normal and BC Tissue Based on Near-Infrared Spectroscopy," *IEEE Transactions on Biomedical Circuits and Systems*, vol. 14, no. 4, pp. 879-888, Aug. 2020.
doi: 10.1109/TBCAS.2020.3005971
 17. R. K. Samala, H. -P. Chan, L. Hadjiiski, M. A. Helvie, C. D. Richter and K. H. Cha, "BC Diagnosis in Digital Breast Tomosynthesis: Effects of Training Sample Size on Multi-Stage Transfer Learning Using Deep Neural Nets," *IEEE Transactions on Medical Imaging*, vol. 38, no. 3, pp. 686-696, March 2019.
doi: 10.1109/TMI.2018.2870343
 18. G. Li, C. Li, G. Wu, D. Ji and H. Zhang, "Multi-View Attention-Guided Multiple Instance Detection Network for Interpretable BC Histopathological Image Diagnosis," *IEEE Access*, vol. 9, pp. 79671-79684, 2021.
doi: 10.1109/ACCESS.2021.3084360
 19. P. Baran et al., "High-Resolution X-Ray Phase-Contrast 3-D Imaging of Breast Tissue Specimens as a Possible Adjunct to Histopathology," *IEEE Transactions on Medical Imaging*, vol. 37, no. 12, pp. 2642-2650, Dec. 2018.
doi: 10.1109/TMI.2018.2845905
 20. J. Zheng, D. Lin, Z. Gao, S. Wang, M. He and J. Fan, "Deep Learning Assisted Efficient AdaBoost Algorithm for BC Detection and Early Diagnosis," *IEEE Access*, vol. 8, pp. 96946-96954, 2020.
doi: 10.1109/ACCESS.2020.2993536
 21. Z. Wang et al., "BC Detection Using Extreme Learning Machine Based on Feature Fusion With CNN Deep Features," *IEEE Access*, vol. 7, pp. 105146-105158, 2019.
doi: 10.1109/ACCESS.2019.2892795
 22. X. Zhang et al., "Deep Learning Based Analysis of BC Using Advanced Ensemble Classifier and Linear Discriminant Analysis," *IEEE Access*, vol. 8, pp. 120208-120217, 2020.
doi: 10.1109/ACCESS.2020.3005228
 23. Y. Yari, T. V. Nguyen and H. T. Nguyen, "Deep Learning Applied for Histological Diagnosis of BC," *IEEE Access*, vol. 8, pp. 162432-162448, 2020.
doi: 10.1109/ACCESS.2020.3021557
 24. G. Ma and M. Soleimani, "Spectral Capacitively Coupled Electrical Resistivity Tomography for BC Detection," *IEEE Access*, vol. 8, pp.

- 50900-50910, 2020.
doi: 10.1109/ACCESS.2020.2980112
25. J. Teng et al., "Bayesian Inference of Lymph Node Ratio Estimation and Survival Prognosis for BC Patients," *IEEE Journal of Biomedical and Health Informatics*, vol. 24, no. 2, pp. 354-364, Feb. 2020.
doi: 10.1109/JBHI.2019.2943401
26. D. A. Zebari, D. Q. Zeebaree, A. M. Abdulazeez, H. Haron and H. N. A. Hamed, "Improved Threshold Based and Trainable Fully Automated Segmentation for BC Boundary and Pectoral Muscle in Mammogram Images," *IEEE Access*, vol. 8, pp. 203097-203116, 2020.
doi: 10.1109/ACCESS.2020.3036072
27. M. K. Bhowmik, U. R. Gogoi, G. Majumdar, D. Bhattacharjee, D. Datta and A. K. Ghosh, "Designing of Ground-Truth-Annotated DBT-TU-JU Breast Thermogram Database Toward Early Abnormality Prediction," *IEEE Journal of Biomedical and Health Informatics*, vol. 22, no. 4, pp. 1238-1249, July 2018.
doi: 10.1109/JBHI.2017.2740500
28. X. Tang, L. Cai, Y. Meng, C. Gu, J. Yang and J. Yang, "A Novel Hybrid Feature Selection and Ensemble Learning Framework for Unbalanced Cancer Data Diagnosis With Transcriptome and Functional Proteomic," *IEEE Access*, vol. 9, pp. 51659-51668, 2021.
doi: 10.1109/ACCESS.2021.3070428
29. G. G. N. Geweid and M. A. Abdallah, "A Novel Approach for BC Investigation and Recognition Using M-Level Set-Based Optimization Functions," *IEEE Access*, vol. 7, pp. 136343-136357, 2019.
doi: 10.1109/ACCESS.2019.2941990
- A. H. Osman and H. M. A. Aljahdali, "An Effective of Ensemble Boosting Learning Method for BC Virtual Screening Using Neural Network Model," *IEEE Access*, vol. 8, pp. 39165-39174, 2020.
doi: 10.1109/ACCESS.2020.2976149
30. Dataset 1 is downloaded from :”
<http://peipa.essex.ac.uk/info/mias.html>”,
Access Date: 2021-09-06
31. J. Subramaniam, R. J. Kannan and D. Ebenezer, "Parallel and Pipelined 2-D Median Filter Architecture," *IEEE Embedded Systems Letters*, vol. 10, no. 3, pp. 69-72, Sept. 2018, doi: 10.1109/LES.2017.2771453.
32. Li Wenchao, Z. Yong and X. Shixiong, "A Novel Clustering Algorithm Based on Hierarchical and K-means Clustering," 2007 Chinese Control Conference, 2007, pp. 605-609, doi: 10.1109/CHICC.2006.4347538.
33. X. Liu, F. Xue and L. Teng, "Surface Defect Detection Based on Gradient LBP," 2018 IEEE 3rd International Conference on Image, Vision and Computing (ICIVC), 2018, pp. 133-137, doi: 10.1109/ICIVC.2018.8492798.
34. R. Cristin, Dr. V. Cyril Raj and Ramalatha Marimuthu, "Face Image Forgery Detection by Weight Optimized Neural Network Model", *Multimedia Research*, Vol.2, No.2, pp.19-27, 2019.
35. Ayesha Hojage, "Race Detection using Mutated Salp Swarm Optimization Algorithm based DBN from Face Shape Features", *Multimedia Research*, Vol. 4, Issue 2, 2021.
36. Chithra R S, Jagatheeswari P, "Enhanced WOA and Modular Neural Network for Severity Analysis of Tuberculosis", *Multimedia Research*, Vol.2, No.3, pp.43-55, 2019.
37. Mohammad Dehghani and Pavel Trojovský, "Teamwork Optimization Algorithm: A New Optimization Approach for Function Minimization/Maximization", *Sensors*, 2021